

1 **The photoreceptor UVR8 mediates the perception of both UV-B and UV-A wavelengths up to**
2 **350 nm of sunlight with responsivity moderated by cryptochromes**

3

4 Neha Rai¹, Andrew O'Hara², Daniel Farkas², Omid Safronov¹, Khuanpiroon Ratanasopa², Fang
5 Wang¹, Anders V. Lindfors³, Gareth I. Jenkins⁴, Tarja Lehto⁵, Jarkko Salojärvi^{1,6}, Mikael Brosché¹,
6 Åke Strid², Pedro J. Aphalo^{1*}, Luis O. Morales^{1†*}

7

8 ¹Organismal and Evolutionary Biology, Faculty of Biological and Environmental Sciences, and
9 Viikki Plant Science Centre, University of Helsinki, 00014 Helsinki, Finland;

10 ²School of Science and Technology, Örebro Life Science Center, Örebro University, 70182 Örebro,
11 Sweden;

12 ³Finnish Meteorological Institute, Meteorological Research, 00101 Helsinki, Finland;

13 ⁴Institute of Molecular, Cell and Systems Biology, College of Medical, Veterinary and Life
14 Sciences, University of Glasgow, Glasgow G12 8QQ, United Kingdom;

15 ⁵School of Forest Sciences, University of Eastern Finland, 80101 Joensuu, Finland;

16 ⁶School of Biological Sciences, Nanyang Technological University, 637551 Singapore, Singapore

17

18 [†]Current address: School of Science and Technology, Örebro Life Science Center, Örebro
19 University, 70182 Örebro, Sweden

20 * These authors contributed equally as senior authors.

21

22 Author for correspondence:

23 *Luis O. Morales*

24 *Tel: +46739434429*

25 *Email: luis.morales@oru.se*

26 *ORCID: [0000-0002-9233-7254](https://orcid.org/0000-0002-9233-7254)*

27

28 **Funding**

29

30 Funding by Academy of Finland (252548) to PJA, and (307335) to MB and JS; EDUFI Fellowship,
31 Finnish Cultural Foundation and Doctoral Program in Plant Sciences funding (University of
32 Helsinki) to NR; Knowledge foundation (20130164) and Swedish Research Council Formas (942-
33 2015-516) to ÅS; Strategic Young Researchers Recruitment Programme (Örebro University) to
34 LOM.

35

36 **Abstract**

37

38 The photoreceptors UV RESISTANCE LOCUS 8 (UVR8) and CRYPTOCHROMES 1 and 2
39 (CRYs) play major roles in the perception of UV-B (280–315 nm) and UV-A/blue radiation (315–
40 500 nm), respectively. However, it is poorly understood how they function in sunlight. The roles of
41 UVR8 and CRYs were assessed in a factorial experiment with *Arabidopsis thaliana* wild-type and
42 photoreceptor mutants exposed to sunlight for 6 h or 12 h under five types of filters with cut-offs in
43 UV and blue-light regions. Transcriptome-wide responses triggered by UV-B and UV-A
44 wavelengths shorter than 350 nm (UV-A_{sw}) required UVR8 whereas those induced by blue and UV-
45 A wavelengths longer than 350 nm (UV-A_{lw}) required CRYs. UVR8 modulated gene expression in
46 response to blue light while lack of CRYs drastically enhanced gene expression in response to UV-
47 B and UV-A_{sw}. These results agree with our estimates of photons absorbed by these photoreceptors
48 in sunlight and with *in vitro* monomerization of UVR8 by wavelengths up to 335 nm. Motif
49 enrichment analysis predicted complex signaling downstream of UVR8 and CRYs. Our results
50 highlight that it is important to use UV waveband definitions specific to plants'
51 photomorphogenesis as is routinely done in the visible region.

52

53 **Keywords**

54

55 *Arabidopsis thaliana*, blue light, cryptochrome, gene expression, photoreceptor interaction, solar
56 radiation, ultraviolet radiation, UVR8.

57

58 **Acknowledgements**

59

60 We acknowledge Petri Auvinen (University of Helsinki) for RNA-sequencing.

61

62 **Conflict of Interest**

63

64 The authors declare no conflict of interests.

65 **Main text file**

66

67 **The photoreceptor UVR8 mediates the perception of both UV-B and UV-A wavelengths up to**
68 **350 nm of sunlight with responsivity moderated by cryptochromes**

69

70 **Abstract**

71

72 The photoreceptors UV RESISTANCE LOCUS 8 (UVR8) and CRYPTOCHROMES 1 and 2
73 (CRYs) play major roles in the perception of UV-B (280–315 nm) and UV-A/blue radiation (315–
74 500 nm), respectively. However, it is poorly understood how they function in sunlight. The roles of
75 UVR8 and CRYs were assessed in a factorial experiment with *Arabidopsis thaliana* wild-type and
76 photoreceptor mutants exposed to sunlight for 6 h or 12 h under five types of filters with cut-offs in
77 UV and blue-light regions. Transcriptome-wide responses triggered by UV-B and UV-A
78 wavelengths shorter than 350 nm (UV-A_{sw}) required UVR8 whereas those induced by blue and UV-
79 A wavelengths longer than 350 nm (UV-A_{lw}) required CRYs. UVR8 modulated gene expression in
80 response to blue light while lack of CRYs drastically enhanced gene expression in response to UV-
81 B and UV-A_{sw}. These results agree with our estimates of photons absorbed by these photoreceptors
82 in sunlight and with *in vitro* monomerization of UVR8 by wavelengths up to 335 nm. Motif
83 enrichment analysis predicted complex signaling downstream of UVR8 and CRYs. Our results
84 highlight that it is important to use UV waveband definitions specific to plants’
85 photomorphogenesis as is routinely done in the visible region.

86

87 **Keywords**

88

89 *Arabidopsis thaliana*, blue light, cryptochrome, gene expression, photoreceptor interaction, solar
90 radiation, ultraviolet radiation, UVR8.

91

92 **1 INTRODUCTION**

93

94 Sunlight regulates plant growth, development and acclimation to the environment, while responses
95 to specific wavelengths are regulated by different photoreceptors. The contribution of different
96 wavelengths of sunlight to plant responses depends both on the optical properties of the
97 photoreceptors and on the spectrum and photon irradiance of the incident radiation. Research under
98 controlled conditions has shown that the photoreceptors UV RESISTANCE LOCUS 8 (UVR8) and

99 CRYPTOCHROMES 1 and 2 (CRYs) play major roles in the perception of UV-B (ground level
100 290–315 nm) and UV-A/blue radiation (315–500 nm), respectively (Ahmad & Cashmore, 1993;
101 Lin, 2000; Yu *et al.*, 2010; Rizzini *et al.*, 2011). However, in sunlight, the irradiances of
102 photosynthetically active radiation (PAR, 400–700 nm) and UV-A (315–400 nm) relative to UV-B
103 are much higher than those normally used in controlled environments making it necessary to assess
104 which wavelengths are effectively perceived by UVR8 and CRYs in sunlight.

105

106 Indoor and outdoor experiments with UV-B irradiances similar to those in sunlight have shown that
107 UVR8 can regulate transcript abundance of hundreds of genes, including those involved in UV
108 protection, photo-repair of UV-B-induced DNA damage, oxidative stress and several transcription
109 factors (TFs) shared with other signaling pathways (Brown *et al.*, 2005; Favory *et al.*, 2009;
110 Morales *et al.*, 2013). The first step in this response is the absorption of UV-B photons by UVR8
111 which triggers a change in conformation from homodimer to monomer enhancing its accumulation
112 in the nucleus (Brown *et al.*, 2005; Kaiserli & Jenkins, 2007; Rizzini *et al.*, 2011). Downstream
113 signaling depends on UVR8 monomers binding to CONSTITUTIVE PHOTOMORPHOGENIC 1
114 (COP1) (Favory *et al.*, 2009), thereby inactivating the E3 ubiquitin ligase activity of COP1. The
115 UVR8-COP1 association stabilizes the TF ELONGATED HYPOCOTYL 5 (HY5), a master
116 regulator of photomorphogenesis in plants (Favory *et al.*, 2009; Huang *et al.*, 2013; Gangappa &
117 Botto, 2016). Both HY5 and HY5 HOMOLOG (HYH) have been identified as key TFs regulating
118 the expression of most genes responding to UV-B through UVR8 signaling (Brown & Jenkins,
119 2008; Favory *et al.*, 2009). Moreover, UVR8 directly interacts with WRKY DNA-BINDING
120 PROTEIN 36 (WRKY36), BRI1-EMS-SUPPRESSOR1 (BES1) and BES1-INTERACTING MYC-
121 LIKE 1 (BIM1) TFs to regulate transcription (Liang *et al.*, 2018; Yang *et al.*, 2018). UV-B radiation
122 induces the expression of genes encoding REPRESSOR OF UV-B PHOTOMORPHOGENESIS 1
123 (RUP1) and RUP2 proteins, which interact with UVR8 directly and convert the active monomers
124 into homodimers, thereby decreasing the abundance of UVR8 monomers through negative feedback
125 (Gruber *et al.*, 2010; Heijde & Ulm, 2013). Because indoor studies are often done using
126 unrealistically high UV-B:PAR and low UV-A:PAR ratios, the participation of UVR8 in the
127 regulation of the transcriptome in response to UV-B, UV-A and blue wavelengths of solar radiation
128 remains uncertain.

129

130 Our understanding of the molecular mechanisms underpinning CRY-mediated responses to blue
131 light is far better than for those to UV-A. In indoor experiments with blue light, CRYs have been
132 found to regulate photomorphogenesis and expression of genes involved in light signaling,

133 photosynthetic light reaction, the Calvin cycle, phenylpropanoid metabolic pathway and stress
134 response (Ohgishi *et al.*, 2004; Kleine *et al.*, 2007). Upon absorption of blue light photons, CRYs
135 alter conformation from monomers to homodimers and oligomers (Wang *et al.*, 2016). CRYs
136 homodimers or oligomers interact with COP1 and SUPPRESSOR OF PHY A (SPA) proteins
137 through various mechanisms (Yang *et al.*, 2001; Wang *et al.*, 2001; Lian *et al.*, 2011; Liu *et al.*,
138 2011b; Zuo *et al.*, 2011; Podolec & Ulm, 2018). These interactions stabilize HY5 abundance and
139 consequent transcriptional regulation (Liu *et al.*, 2011a; Yang *et al.*, 2017; Podolec & Ulm, 2018).
140 CRYs also interact directly with TFs such as BES1, BIM1, CRYPTOCHROME-INTERACTING
141 basic helix-loop-helix 1 (CIB1), PHYTOCHROME-INTERACTING FACTOR 4 (PIF4) and PIF5
142 regulating transcription (Liu *et al.*, 2008; Pedmale *et al.*, 2016; Wang *et al.*, 2018). Thus, both
143 UVR8 and CRY signaling share some TFs such as HY5, HYH and BES1 suggesting the possibility
144 of crosstalk. Despite these studies under controlled conditions, the participation of CRYs in the
145 regulation of the transcriptome in sunlight remains poorly understood due to the unrealistic light
146 conditions used.

147

148 As photoreceptors have broad peaks of absorption, their absorption spectra partially overlap. Both
149 CRYs and UVR8 absorb in the UV-B region, while CRYs also absorb strongly at longer
150 wavelengths (Banerjee *et al.*, 2007; Christie *et al.*, 2012; Yang *et al.*, 2015). Given the overlapping
151 spectra of photoreceptors and the fact that plants are simultaneously exposed to all wavelengths of
152 sunlight, only research in sunlight can assess the roles of photoreceptors in nature. The available
153 absorption spectrum for the UVR8 molecule covers the UV-C and UV-B regions, extending only
154 15 nm into the UV-A (Christie *et al.*, 2012) making even speculations about the possible role of
155 UVR8 in the UV-A region uncertain. Furthermore, our previous studies indicated that different
156 regions within UV-A could trigger different responses to metabolite accumulation and transcript
157 abundance of selected genes (Siipola *et al.*, 2015; Rai *et al.*, 2019). Besides, results from an indoor
158 experiment suggested the participation of UVR8 in flavonoid accumulation in response to UV-A
159 from LEDs (Brelsford *et al.*, 2018). However, it is not yet clear which UV-A wavelengths are
160 perceived through UVR8 and which ones through CRYs.

161

162 To assess the roles of UVR8 and CRYs in the perception of solar UV-B, UV-A and blue radiation,
163 we measured transcriptome-wide responses in Arabidopsis plants exposed to sunlight. We also
164 measured the *in vitro* absorption spectrum of UVR8 in the UV-C, UV-B, UV-A and visible regions
165 (250–500 nm), the *in vitro* monomerization of UVR8 by different UV-A wavelengths, and
166 estimated numbers of sunlight photons absorbed by UVR8 and CRYs. We tested four hypotheses:

167 1) the perception of solar UV-B and UV-A wavelengths up to 350 nm (UV-A_{sw}) is through UVR8,
168 2) the perception of solar UV-A wavelengths above 350 nm (UV-A_{lw}) and blue light is through
169 CRYs, 3) crosstalk between UV-B/UV-A_{sw} and UV-A_{lw}/blue light signaling is asymmetric in plants
170 exposed to sunlight, and 4) gene expression responses to different wavelengths of sunlight are
171 coordinated by multiple TFs resulting in multiple patterns of expression.

172

173 **2 MATERIALS AND METHODS**

174

175 **2.1 Plant material and treatments**

176

177 *Arabidopsis thaliana* ecotype Landsberg *erecta* (*Ler*) and the photoreceptor mutants *uvr8-2* (Brown
178 *et al.*, 2005) and *cry1cry2* (Neff & Chory, 1998) were used. The *uvr8-2* genotype carries a mutation
179 in the C-terminus of the UVR8 protein that impairs signaling in response to UV-B (Cloix *et al.*,
180 2012). The *cry1cry2* genotype carries null mutations for CRY1 and CRY2 protein and consequently
181 is impaired in blue light perception through CRYs (Mazzella *et al.*, 2001). Seeds from different
182 genotypes used in the experiments were previously grown and harvested under the same growth
183 conditions. Seeds were sown in plastic pots (8 cm × 8 cm) containing a 1:1 mixture of peat and
184 vermiculite and kept in darkness at 4 °C for 3 d. Subsequently, the pots were transferred to
185 controlled-environment growth room at 23 °C:19 °C and 70%:90% relative humidity (light:dark)
186 under 12 h photoperiod with 280 μmol m⁻² s⁻¹ white light irradiance, 12 mol day⁻¹ (Osram T8 L
187 36W/865 Lumilux). Rosco filter E-color 226 was used to block the small amount of UV-A radiation
188 emitted by the lamps. Four seedlings of the same genotype were transplanted into each plastic pot
189 (8 cm × 8 cm). After transplanting, plants were kept for 14 d in the same growth room and
190 conditions.

191

192 For exposure to sunlight, plants were moved to the field (Viikki campus, University of Helsinki,
193 60°13'N, 25°1'E) on 21 August 2014 between 07:30 and 08:15. Five treatments were created with
194 different plastic sheets (3 mm thick) and a film (0.12 mm thick) used as long-pass optical filters to
195 selectively exclude different wavebands of the UV and blue regions (Figure 1, Methods S1). The
196 filters were kept 10–15 cm above the top of the plants, on their south and north edges, respectively.
197 Their transmittance was measured with a spectrophotometer (model 8453, Agilent, Waldbronn,
198 Germany, Figure 1). Treatments were randomly assigned within four blocks (biological replicates).
199 One tray was kept under one filter and there was one filter of each type per block. Each tray

200 contained two pots per genotype, positioned at random within the trays, for sampling after 6 h and
201 12 h.

202

203 **2.2 Light conditions and sampling outdoors**

204

205 Hourly solar spectra at ground level were modeled for the 12 h of exposure period using a radiation
206 transfer model (libradtran, Emde *et al.*, 2016) and cloudiness estimates derived from global
207 radiation measurements (Lindfors *et al.*, 2009). Figure S1 shows the solar spectrum at different
208 times of the day when plants were moved outdoors. Figure S2 shows the hourly mean photon
209 irradiance of UV-B (290–315 nm), UV-A_{sw} (315–350 nm), UV-A long-wavelength (UV-A_{lw} 350–
210 400 nm), blue (400–500 nm) and PAR (400–700 nm), for the broader wavebands $\lambda < 350$ nm (290–
211 350 nm) and $\lambda > 350$ nm (350–500 nm). The hourly solar spectra were convoluted by the spectral
212 transmittance of each filter to estimate the spectrum the plants were exposed to. Then these spectra
213 were convoluted by the *in vitro* spectral absorbance of UVR8 (see Results) or of light-adapted
214 CRY2 (Banerjee *et al.*, 2007) to estimate the relative numbers of photons absorbed by UVR8 and
215 CRY2 in each treatment. Plotting and calculations on the simulated spectra were done in R (R Core
216 Team, 2018, Aphalo, 2015).

217

218 Samples were collected after 6 h and 12 h of exposure to sunlight (13:30–14:15, 19:30–20:20) by
219 block with treatments and genotypes in random order within each block. Each biological sample
220 consisted of leaves from four pooled rosettes from the same pot, which were immediately frozen in
221 liquid nitrogen and later stored at -80 °C. Each pooled sample was ground with mortar and pestle in
222 liquid nitrogen.

223

224 **2.3 RNA sequencing**

225

226 Total RNA was extracted from ground leaf samples with a GeneJET Plant RNA Purification Kit
227 following manufacturer's guidelines (Thermo Fisher Scientific, Vilnius, Lithuania). RNA quality
228 was checked with Agilent 2100 Bioanalyzer (Santa Clara, CA, USA) and RNA concentration was
229 measured with ND-1000 Spectrophotometer (NanoDrop Technologies, Thermo Fisher Scientific,
230 Waltham, MA, USA). For RNA-seq measurements, RNA extracts from two pairs of biological
231 replicates were combined into two pooled replicates. Libraries were constructed using TruSeq
232 Stranded mRNA Sample PrepKit (Illumina, San Diego, CA, USA) following manufacturer's

233 instructions. The library concentration was measured using Qubit Fluorometer (Life Technologies,
234 Carlsbad, CA, USA), and quality and size were checked by Fragment Analyzer (Agilent
235 Technologies). Libraries were sequenced on NextSeq 500 (Illumina) generating single end 75 bp
236 reads. RNA-seq raw data was deposited at Gene Expression Omnibus (accession number
237 GSE117199).

238

239 RNA-seq data analysis was done using the JAVA-based client-server system, Chipster (Kallio *et al.*,
240 *et al.*, 2011) and in R. The quality of raw reads was checked with FastQC (Andrews, 2014). Removal
241 of adapter sequences, trimming and cropping of the reads were done using Trimmomatic-0.33
242 (Bolger *et al.*, 2014) in single-end mode. The bases with a Phred score < 20 were trimmed from the
243 ends of the reads, and the reads shorter than 30 bases were removed from the analysis (-Phred33,
244 TRAILING:20, MINLEN:30).

245

246 Filtered reads were mapped to the Arabidopsis transcript reference database AtRTD2 (Zhang *et al.*,
247 2017) using Kallisto V-0.43.0 (CMD:quant) (Bray *et al.*, 2016) with 4000 bootstrap sets. The raw
248 count tables for the two pooled replicates were obtained as the mean of the bootstrap runs. Genes
249 with less than five counts in all 21 filter-treatment \times genotype combinations were removed. The
250 count tables were analyzed for differential gene expression with edgeR 3.24.3 (Robinson *et al.*,
251 2010). The glmLRT (McCarthy *et al.*, 2012) method was used to fit the statistical model separately
252 to data from each genotype. Differentially expressed genes (DEGs) across treatments and
253 photoreceptor mutants under selected pairwise contrasts were assessed with method
254 decideTestsDGE using Benjamini-Hochberg FDR correction of P -values, with $FDR \leq 0.05$. In a
255 separate step, $|\log_2 FC| > \log_2(1.5)$ was used as threshold. Effects of wavebands were assessed by
256 comparing responses between pairs of filters as described above (Figure 1).

257

258 Function plotMDS from package limma 3.38.3 (Ritchie *et al.*, 2015) was used to carry out
259 dimensionality reduction to test for consistency between replicates. To compare RNA-seq and qRT-
260 PCR estimates of transcript abundance, estimates from RNA-seq were re-expressed relative to *Ler*
261 UV0 to match qRT-PCR data and major axis regression applied (R package lmodel2 1.7-3,
262 Legendre, 2018).

263

264 Enrichment of Kyoto Encyclopedia of Genes and Genomes (KEGG) pathways was assessed using
265 function topKEGG (edgeR 3.24.3) using pathway definitions downloaded from <http://rest.kegg.jp>
266 on 10 April 2019. Pathways whose definition included at least 15 but not more than 250 genes were

267 included in the analysis. The enrichments were tested for all lists of DEGs from the contrast tests
268 described above, and all the genes expressed in our experiment were used as background.
269 Conditions used to assess significance of pathway enrichment were P -value cut-off of 0.01 and at
270 least 1/3 of pathway genes differentially expressed. All pathways fulfilling both conditions in at
271 least one treatment contrast are reported.

272

273 **2.4 Cis-motif enrichment**

274

275 Transcription factor binding motifs were collected in the form of position-specific weight matrices
276 (PSWMs) from JASPAR 2018 (Khan *et al.*, 2018) and Cistrome (O'Malley *et al.*, 2016) databases.
277 In addition to PSWMs we analyzed a previously collected set of binding motifs (Blomster *et al.*,
278 2011). For each contrast within each genotype, the enrichment analyses were run on the lists of
279 upregulated and downregulated genes from RNA-seq analysis. The promoter sequences 1000 base
280 pairs upstream of transcription start sites of all Arabidopsis genes were scanned for binding motifs.
281 The regular expressions were matched in R, and PSWM hits were identified using MEME
282 (Ambrosini *et al.*, 2018) with default thresholds. The significance of the overlap between the gene
283 lists and motif occurrences was then tested with Fisher exact test, followed by FDR correction using
284 Benjamini-Hochberg correction. Based on the motifs enriched in each of the separate lists of up or
285 downregulated genes for the 12 waveband \times genotype combinations, we identified putative TFs
286 which could regulate the expression of those genes. Clustering was done over the obtained lists of
287 TFs, based on the adjusted P -values for enrichment in each contrast and genotype combination. For
288 visualization, the P -values were first restricted to the range of 1 to 10^{-4} by converting all smaller
289 values to 10^{-4} , and subsequently applying a \log_{10} transformation. Clustering and plotting of the
290 heatmaps was done with R package pheatmap 1.0.12 (Kolde, 2019). The cut point at 12 clusters was
291 subjectively chosen for plotting; cutting introduces visual breaks without changing the cluster tree
292 or the heatmap in any other way. The ordering of the tree was done with R package dendsort 0.3.3
293 (Sakai *et al.*, 2014).

294

295 **2.5 Quantitative real-time PCR and data analysis**

296

297 Transcript abundance of selected genes was measured with qRT-PCR from four biological
298 replicates and collected both at 6 h and 12 h. At 6 h the same RNA extracts were used for qRT-PCR
299 as for RNA-seq, but without pooling. The qRT-PCR was done according to Rai *et al.* (2019) using

300 primers listed in Table S1. In every run, normalized expression values were scaled to sample *Ler* λ
301 > 400 nm, \log_{10} transformed, and exported from qbase^{PLUS} for statistical analyses in R. Linear
302 mixed-effect models with block as a random factor were fitted using function lme from package
303 ‘nlme’ 3.1-137 (Pinheiro *et al.*, 2018). Factorial ANOVA was used to assess the significance of the
304 main effects (treatment, genotype and exposure time) and of the interactions (treatment \times genotype,
305 treatment \times exposure time, genotype \times exposure time, and treatment \times genotype \times exposure time).
306 Function fit.contrast from package gmodels 2.18.1 (Warnes *et al.*, 2018) was used to fit pairwise
307 contrasts defined *a priori* and *P*-values adjusted with function p.adjust in R (Holm, 1979). Figures
308 were plotted using R package ggplot2 3.1.0 (Wickham, 2009).

309

310 **2.6 In vitro absorption spectra of UVR8 protein**

311

312 Recombinant UVR8 was produced and isolated from *Escherichia coli* with small variations from
313 the original procedure described by Wu *et al.* (2012). The *E. coli* codon-optimized gene for
314 Arabidopsis UVR8 was introduced into the pET11a expression vector generating a construct
315 carrying an N-terminal 6 \times His-tag (Genscript). The construct was verified by DNA-sequencing and
316 transformed into the *E. coli* expression host strain BL21. For the recombinant production of
317 functional UVR8, the N-terminal 6 \times His-tagged UVR8 was overexpressed overnight at 18 °C using
318 0.2 mM β -d-thiogalactopyranoside for induction (Wu *et al.*, 2012). Following the overnight
319 induction, cells were harvested by centrifugation and flash-frozen in liquid nitrogen after which cell
320 pellets were stored at -80 °C. Upon purification of recombinant UVR8, cells were lysed by
321 sonication and soluble protein was separated from insoluble fractions by centrifugation. Further
322 isolation of His-tagged UVR8 was accomplished by immobilized metal-affinity chromatography
323 using a two segmented linear gradient of imidazole. Eluted fractions containing UVR8 was further
324 purified to homogeneity using size-exclusion chromatography as verified by SDS-PAGE.
325 Functionality was verified by electrophoresis assay and fluorescence quenching as described by Wu
326 *et al.* (2012). The UV/Vis absorbance spectrum of UVR8 protein was measured by a standard
327 protocol using a spectrophotometer (Shimadzu UV-1800). To improve the signal-to-noise ratio for
328 spectral regions covering both long and short wavelengths, two separate data sets were recorded for
329 two concentrations of UVR8 protein, 57.0 μ M and 4.5 μ M, respectively. A 25 mM Tris (pH8),
330 150 mM NaCl buffer solution supplemented with 1 mM Beta-mercaptoethanol was used. Protein
331 concentrations were determined using a theoretical absorption coefficient of 91900 M⁻¹cm⁻¹ at
332 280 nm as determined by the ProtParam data server available through the SIB Swiss Institute of
333 Bioinformatics (Gasteiger *et al.*, 2005).

334

335 **2.7 In vitro monomerization of purified UVR8 protein**

336

337 His-tagged *Arabidopsis thaliana* full-length UVR8 was produced in *Nicotiana benthamiana* after
338 *Agrobacterium tumefaciens* transfection using the pEAQ-HT plasmid (Sainsbury *et al.*, 2009) as
339 expression vector. Purification of UVR8 was accomplished using Ni-NTA immobilized metal-
340 affinity and size-exclusion chromatography. Purified UVR8 protein was exposed to UV
341 wavelengths in a 50 μ l cuvette using a pulsed Opolette 355+UV tunable laser (Opotek Inc. USA)
342 with a thermostatic cuvette holder at 4 °C, as described in Díaz-Ramos *et al.* (2018), using doses
343 between 1.9 and 6.2 μ mol. After exposure, samples were added to 4 \times SDS sample buffer (250 mM
344 Tris-HCl pH 6.8, 2% (w/v) SDS, 20% (v/v) β -mercaptoethanol, 40% (v/v) glycerol, 0.5% (w/v)
345 bromophenol blue) (O'Hara & Jenkins, 2012) and were subsequently analyzed by SDS-PAGE
346 without boiling (Rizzini *et al.*, 2011). Gels were stained with Coomassie blue to visualize the dimer
347 and monomer bands.

348

349 **3 RESULTS**

350

351 **3.1 Gene expression mediated by UVR8 and CRYs after 6 h of sunlight exposure**

352

353 To get full assessment of changes in transcript abundances induced by sunlight, we performed
354 RNA-seq from samples collected after 6 h of exposure of plants to filtered sunlight. RNA-seq
355 libraries from the same genotype and treatment clustered together showing consistency among
356 biological replicates (Figure S3). Furthermore, we validated the expression profiles obtained by
357 RNA-seq with qRT-PCR using 11 genes responsive to UV radiation, and/or blue light, or involved
358 in hormone responses (Table S1). The high positive correlation, $R^2 = 0.85$, between the two
359 methods validates the RNA-seq data (Figure S4).

360

361 As shown in the Venn diagrams (Figure 2a), in wild type *Ler*, out of 3741 DEGs, 2786 responded
362 to blue light (868 UP, 1918 DOWN), 960 to UV-A (406 UP, 554 DOWN) and 653 to UV-B (343
363 UP, 310 DOWN). Only 101 DEGs responded to all three solar wavebands UV-B, UV-A and blue.
364 Moreover, less than half of the DEGs responding to UV-B were specific, as the remaining ones
365 responded also to UV-A, blue or both. In contrast, of the DEGs responding to UV-A or blue, more
366 than half were specific (Figure 2a).

367

368 In *uvr8-2*, out of 2095 DEGs only 53 (35 UP, 18 DOWN) responded to UV-B (Figure **2b**). The
369 number of DEGs responding to UV-A was only 1/3 of that in *Ler* (356 differentially expressed, DE;
370 125 UP, 231 DOWN) while also the number of DEGs responding to blue light was only 2/3 of that
371 in *Ler* (1849 DE; 763 UP, 1086 DOWN) (Figure 2a,b). Furthermore, 1/3 of the DEGs responding to
372 blue in *uvr8-2* were unique and not shared by *Ler* and *cry1cry2* (Figure S5). Thus, the results
373 confirm our hypothesis that UVR8 plays a role in UV-A perception and also indicate that functional
374 UVR8 modulates gene expression responses to solar blue wavelengths.

375

376 In *cry1cry2*, out of 2948 DEGs only 139 (87 UP, 52 DOWN) responded to solar blue light (Figure
377 2c). Surprisingly for this mutant, out of the 2948 DEGs, 1272 (425 UP, 847 DOWN) still responded
378 to UV-A (Figure 2c). Also, the number of DEGs responding to UV-B increased from 653 in *Ler* to
379 2040 (784 UP, 1256 DOWN) in *cry1cry2* (Figure 2a,c).

380

381 To explore the UV-A signaling roles of UVR8 and CRYs in more detail, we next assessed the
382 effects of longer and shorter wavelength regions within UV-A by comparing responses between
383 pairs of filters: UV-A_{sw} (>315 nm vs >350 nm) and UV-A_{lw} (>350 nm vs >400 nm) (Figure 1). In
384 *Ler*, out of 190 DEGs, 166 responded to UV-A_{sw} (113 UP, 53 DOWN) and only 26 to UV-A_{lw} (16
385 UP, 10 DOWN), with only 2 DEGs shared between the two treatments (Figure 3a). In *uvr8-2*, out of
386 77 DEGs, 7 (3 UP, 4 DOWN) responded to UV-A_{sw}, while 72 (17 UP, 55 DOWN) to UV-A_{lw}
387 (Figure 3b). In *cry1cry2*, out of 1057 DEGs, 1050 (340 UP, 710 DOWN) responded to UV-A_{sw} and
388 only 16 (8 UP, 8 DOWN) to UV-A_{lw} (Figure 3c). The number of DEGs responding to UV-A_{sw} in
389 *cry1cry2* was more than six times those responding to UV-A_{sw} in *Ler*, a similar but stronger effect
390 to that of UV-B (Figure 3a,c). Furthermore, 3/4 and 9/10 of the DEGs responding to UV-B and UV-
391 A_{sw}, respectively, in *cry1cry2* were unique and not shared by *Ler* or *uvr8-2* (Figure S5). Here, it
392 should be noted that the individual numbers of DEGs under UV-A_{sw} and UV-A_{lw} add up to a
393 smaller number than the number of DEGs for whole UV-A region (315–400 nm) (cf. Figures 3 and
394 2). This difference mainly arises from statistically comparing pairs of treatments that correspond to
395 smaller (UV-A_{sw} and UV-A_{lw}) or larger (whole UV-A) amounts of sunlight attenuation.

396

397 We next tested whether the requirement of UVR8 vs CRYs observed within the UV-A remained
398 valid when including wavelengths in the UV-B and blue bands in the analysis. For this test, DEGs
399 responding to $\lambda < 350$ nm (contrast between >290 nm vs >350 nm) and $\lambda > 350$ nm (contrast
400 between >350 nm vs >500 nm) were quantified (Figure 4). The number of DEGs responding to $\lambda <$
401 350 nm in *uvr8-2* drastically decreased to 1/37 of those in *Ler* while the number of those

402 responding in *cry1cry2* increased to 2.7 times of those in *Ler*. The number of DEGs responding to λ
403 > 350 nm in *cry1cry2* decreased to 1/35 of those in *Ler*, while the number of those responding in
404 *uvr8-2* also decreased but only to 4/5 of those in *Ler* (Figure 4). This test indicates that in sunlight
405 functional UVR8 is required for transcriptome-wide response to $\lambda < 350$ nm and CRYs are required
406 for those to $\lambda > 350$ nm and that functional CRYs antagonize this transcriptome-wide response to λ
407 < 350 nm.

408

409 Our lists of DEGs for the 12 waveband-contrast \times genotype combinations were enriched for 45
410 KEGG metabolic pathways in total (Figure S6a-c). The analysis showed that UVR8 mediated the
411 expression of genes involved in all enriched metabolic processes induced by UV-B and UV-A_{sw} in
412 *Ler* and *cry1cry2*. Since the flavonoid biosynthesis pathway was still enriched in *uvr8-2* by UV-B,
413 dependence on UVR8 was partial (Figure S6a,b). Expression of genes involved in ribosome
414 biogenesis, protein processing and endocytosis under solar blue required functional UVR8 (Figure
415 S6a,b). CRYs mediated the expression of genes involved in most metabolic pathways regulated by
416 blue light in *Ler* and *uvr8-2*, as these responses were missing in *cry1cry2*. The cases where the
417 response to blue light was not fully dependent on CRYs were flavonoid biosynthesis, diterpenoid
418 biosynthesis, phenylalanine metabolism, circadian rhythm, vitamin B6 metabolism,
419 phenylpropanoid biosynthesis. Strikingly, many pathways including photosynthesis, glucosinolates
420 biosynthesis, and plant hormone signal transduction were over-represented in *cry1cry2* compared to
421 *Ler* in response to UV-B and UV-A_{sw} (Figure S6a,c).

422

423 **3.2 Photon absorption and monomerization of UVR8**

424

425 To evaluate whether the actions of UVR8 and CRYs at $\lambda < 350$ nm and $\lambda > 350$ nm are consistent
426 with their absorption spectra, we estimated the relative number of photons absorbed by both
427 photoreceptors given the solar spectral irradiance on the sampling day under each filter (Figure 5).
428 For UVR8 we used a newly measured absorption spectrum extending into the visible region (Figure
429 S7), while for CRYs we used a published absorption spectrum for CRY2 (Banerjee *et al.*, 2007). As
430 a result of the shape of the solar spectrum, the estimates showed that UV-A_{sw} was the band where
431 UVR8 was predicted to absorb most photons. Relative to these maxima, UVR8 was predicted to be
432 the main UV-A_{sw} photoreceptor. In the UV-A_{lw} our estimates showed that both CRYs and UVR8
433 absorbed a large number of photons (Figure 5). While UVR8 absorbed a considerable number of
434 blue photons, CRY2 absorbed very few UV-B photons.

435

436 As monomerization of UVR8 is required for UV-B signaling (Rizzini *et al.*, 2011), we assessed *in*
437 *vitro* if laser radiation of different wavelengths within the UV-B and UV-A bands can monomerize
438 purified UVR8 protein. We found that UVR8 monomerized in response to UV wavelengths in the
439 range 300–335 nm but not in 340–350 nm (Figure 6).

440

441 **3.3 Cis-motif enrichment**

442

443 As enrichment of DNA binding motifs can inform about the putative involvement of TFs in the
444 observed gene-expression responses (McLeay & Bailey, 2010), we assessed *in silico* the enrichment
445 of known *cis*-regulatory elements in the promoter regions of the DEGs from each waveband-
446 genotype combination (Figures 7, S8). The analysis identified 187 putative regulatory TFs whose
447 binding motifs were significantly enriched among the DEGs for at least one waveband-genotype
448 combination (Figures 7, S8). The TFs grouped into 12 distinct clusters based on the similarity of
449 their enrichment patterns across four waveband contrasts and three genotypes (Figure 7). Out of
450 these TFs, 53 were themselves differentially expressed. Clusters A, C, D, F, H and I were
451 homogeneous with respect to TF family, whereas the rest were heterogeneous. Within
452 homogeneous clusters several promoter motifs were enriched (Figures 7, S8).

453

454 In cluster A, several MYB TFs including MYB111 were predicted to regulate the expression of
455 genes with increased transcript abundance in response to UV-B and blue in all genotypes, while in
456 response to UV-A_{sw} significant enrichment was found only in *Ler* and *cry1cry2* (cluster A, Figure
457 7). TFs in this group were the only ones enriched for genes responding to UV-B in *uvr8-2*. Out of
458 these seven TFs, four were themselves differentially expressed in response to the treatments.

459

460 HY5, PIF1, PIF3, PIF4, PIF7, BES1 were grouped in cluster B, and were predicted to regulate the
461 expression of genes with increased transcript abundance in response to solar UV-B in *Ler* and
462 *cry1cry2* (Figure 7) and of genes with either increased or decreased transcript abundance in
463 response to solar blue in *Ler* and *uvr8-2*. Most of these same TFs were enriched for two additional
464 responses only in *cry1cry2*: decreased transcript abundance by UV-B and increased transcript
465 abundance by UV-A_{sw}. Out of these 15 TFs, seven, including HY5, PIF1, PIF3, PIF4 and BES1,
466 were themselves differentially expressed. Cluster C which follows a response pattern similar to that
467 of cluster B groups 14 bZIP TFs of which three were differentially expressed.

468

469 Eleven members of HD-ZIP TFs including HAT5 grouped in cluster D and were enriched for
470 decreased transcript abundance only in response to blue light in *Ler* and *uvr8-2* but in response to
471 UV-B and UV-A_{sw} only in *cry1cry2* (Figure 7). Out of these 11 TFs, four including HAT5 were
472 differentially expressed. Cluster E which follows a response pattern similar to that of cluster D
473 contains TFs from a mix of families of which eight were differentially expressed.

474

475 Five GATA TFs were enriched for DEGs repressed by blue only in *Ler* whereas in the other two
476 mutants these TFs were not enriched for any response (cluster F, Figure 7). WRKY TFs were
477 enriched only for DEGs with decreased expression in response to UV-A_{sw} in *cry1cry2* (cluster G).
478 The number of differentially expressed TFs were 1 and 9 in clusters F and G, respectively. The
479 remaining clusters (H-L) showed multiple but poorly defined patterns of enrichment.

480

481 **3.4 Transcript abundance after 6 h and 12 h**

482

483 We used qRT-PCR to determine changes in transcript abundance after 6 h (mid-day) and after 12 h
484 (before sunset) of exposure to filtered solar radiation, allowing the assessment of transcript
485 abundance at two times of the day when solar UV-B:UV-A photon ratio was very different. We
486 tested 11 genes (Figures 8, S9). The three-way interaction, treatment × genotype × exposure time,
487 was significant for four genes: *RUP2* (involved in UVR8 signaling), *CHALCONE SYNTHASE*
488 (*CHS*) and *CHALCONE ISOMERASE (CHI)* (flavonoid biosynthesis); and *SOLANESYL*
489 *DIPHOSPHATE SYNTHASE 1 (SPS1)* (ubiquinone biosynthesis) (Figure 8, Table S2). This
490 indicates that in sunlight the role of UVR8 and CRYs in the regulation of transcript abundance of
491 these genes changed in time. For these four genes across all genotypes, the response to filter
492 treatments at 6 h was stronger than at 12 h.

493

494 Solar UV-B at 6 h increased transcript abundance of *CHI* and *CHS* in all genotypes and of *RUP2* in
495 *Ler* and *cry1cry2* but not in *uvr8-2* (Figure 8). This response to UV-B was stronger in *cry1cry2* than
496 in *Ler* for all these genes. Solar UV-A_{sw} at 6 h increased transcript abundance of *CHI*, *CHS*, *RUP2*
497 and *SPS1* in *Ler* and *cry1cry2* but not in *uvr8-2*. As for UV-B, the transcript abundance response to
498 6 h of UV-A_{sw} was stronger in *cry1cry2* than in *Ler* for these four genes. Both solar UV-B and UV-
499 A_{sw} at 12 h increased the abundance of *CHS*, but only in *cry1cry2*. These results support regulation
500 of transcript abundance by UVR8 in both UV-B and UV-A_{sw}, antagonized by CRYs.

501

502 Solar UV-A_{Iw} at both 6 h and 12 h decreased the transcript abundance of *CHS* in *cry1cry2* (Figure
503 8). UV-A_{Iw} at 12 h increased the transcript abundance of *RUP2* in *Ler* and of *SPS1* in both *Ler* and
504 *uvr8-2* but not in *cry1cry2*. Overall, transcript abundance was less responsive to UV-A_{Iw} than to
505 UV-A_{sw}. Solar blue light at 6 h increased transcript abundance of *CHI*, *CHS* and *RUP2* in all
506 genotypes whereas of *SPS1* in *Ler* and *uvr8-2* but not in *cry1cry2*. Blue light at 12 h increased the
507 abundance of *CHI* and *RUP2* only in *Ler* and *uvr8-2*, and of *CHS* in all three genotypes, but less in
508 *cry1cry2*. These results support regulation of transcript abundance by CRYs in UV-A_{Iw} and blue
509 light.

510

511 **4 DISCUSSION**

512

513 **4.1 Effective range of wavelengths for action of UVR8 and CRYs in sunlight**

514

515 In plant photobiology the consensus has been that UVR8 and CRYs function as UV-B and
516 blue/UV-A photoreceptors, respectively (Ahmad & Cashmore, 1993; Rizzini *et al.*, 2011).
517 However, here we show that UVR8 mediates transcriptome-wide changes in response to both solar
518 UV-A_{sw} and UV-B (Figures 2–4). Assuming that UVR8 monomers are required for signaling and
519 response (Rizzini *et al.*, 2011), for UVR8 to mediate responses to UV-A_{sw} it must absorb enough
520 photons at these longer wavelengths and monomerize. Our *in silico* estimates based on spectral
521 absorbance predict that UVR8 absorbs more UV-A_{sw} photons than UV-B photons in sunlight
522 (Figure 5), because sunlight contains at least 30 times more UV-A_{sw} photons than UV-B photons
523 (Aphalo, 2018). This explains why the role of UVR8 in UV-A_{sw} perception has not been observed
524 in earlier studies using artificial light with unrealistically high UV-B:PAR and low UV-A:PAR
525 ratios. We also show that *in vitro* UVR8 dimers convert to monomers when exposed to radiation of
526 wavelengths between 300 nm and 335 nm but not in response to longer wavelengths (Figure 6). As
527 the UVR8 protein does absorb photons at wavelengths longer than 335 nm, a possible explanation
528 for this transition between 335 nm and 340 nm is a threshold in the energy per photon required for
529 monomerization. The dose we used at 335 nm was more than 3000 times the maximum used by
530 Díaz-Ramos *et al.* (2018), who observed *in vitro* almost complete monomerization at 310 nm, the
531 longest wavelength they investigated.

532

533 We also found that UVR8 affected blue light-induced gene expression, as fewer and in part
534 different genes responded to blue light in *uvr8-2* when compared to *Ler* (Figures 2a,b, S5). This
535 effect was unexpected, as the effect of blue light was assessed in a background of strongly

536 attenuated UV-B and UV-A. Furthermore, KEGG pathway analysis indicates that functional UVR8
537 might be required for blue-light-dependent expression of genes involved in ribosome biogenesis,
538 protein processing and endocytosis (Figures S6a-c). Our estimates also predict that photon
539 absorption by UVR8 in sunlight extends as far as the blue region (Figure S7), where we observed
540 UVR8-dependent modulation of these specific responses to solar blue instead of a clear-cut
541 requirement as at shorter wavelengths. Although evidence for perception of blue light by UVR8 is
542 weak, the lack of monomerization in response to wavelengths longer than 335 nm suggests that
543 photoreception by UVR8 at longer wavelengths would have to depend on a different mechanism.

544

545 Our transcriptomic data at 6 h (solar noon) indicate that CRYs are the main photoreceptors
546 mediating gene expression responses to solar blue and UV-A_{lw}, but not to UV-A_{sw}. This contrasts
547 with the currently accepted role of CRYs in perception of the whole UV-A waveband (Yu *et al.*,
548 2010). Yet, the absence of CRYs increased the number of DEGs up to three times in response to
549 UV-B and up to six times in response to UV-A_{sw} (Figures 2a,c and 3a,c), an unexpectedly large
550 effect affecting many metabolic processes (Figure S6). However, while CRYs absorb comparatively
551 fewer photons at these shorter wavelengths than in the blue, the effect of UV-B and UV-A_{sw}
552 exposure was assessed in a background of UV-A_{lw} and blue radiation, a condition under which
553 CRY signaling was activated in the WT but not in *cry1cry2*. Thus, the previously described
554 negative regulation of four UVR8-mediated genes by CRYs in UV-B and UV-A_{sw} (Rai *et al.*, 2019)
555 was now expanded to the whole transcriptome indicating an interaction between UVR8 and CRYs
556 leading to wide-ranging regulation of primary and secondary metabolism (Figures 2–4, S6).
557 Furthermore, this negative regulation was observed using qRT-PCR at both 6 h and 12 h for *CHS*
558 (Figure 8) indicating that this effect can persist until the end of the photoperiod even though UV-B
559 irradiance was very low at this time, suggesting a carry-over effect. The transcript abundance of
560 *RUP1* and *RUP2* was increased in response to UV-A_{sw} in *cry1cry2* compared to *Ler* (Figure 8),
561 indicating that the crosstalk between UV-B/UV-A_{sw} and UV-A_{lw}/blue signaling pathways may
562 involve RUPs. In addition, a recent study demonstrated that both UVR8 and CRYs use VP motifs to
563 compete for binding the WD40 domain of COP1 (Lau *et al.*, 2019). Therefore, crosstalk between
564 the two signaling pathways could involve COP1. These earlier results together with our new
565 observations provide a good starting point for future studies on the molecular mechanism of
566 interaction between UVR8 and CRYs in sunlight and its relevance to plant adaptation and
567 acclimation to diurnal and seasonal variation in the solar spectrum.

568

569 **4.2 Putative TFs behind different patterns of gene expression response**

570

571 Our promoter enrichment analysis highlights the possible roles of several TFs in controlling the
572 observed gene expression responses downstream of UVR8 and CRYs. The analysis predicted that
573 MYB TFs, known regulators of flavonol accumulation (Stracke *et al.*, 2007), regulate the
574 expression of genes responding to UV-B partially independent of UVR8, and of those responding to
575 UV-A_{sw} through UVR8 (Figure 7, cluster A). The data also show that HAT5 and PIF5 (clusters D,
576 E) are predicted to specifically regulate gene expression in response to solar blue through CRYs.
577 These results in sunlight agree with a previous report where PIF5 is shown to function downstream
578 of CRYs to mediate hypocotyl elongation in response to artificial blue light (Pedmale *et al.*, 2016).

579

580 Although earlier work has emphasized the role of HY5 as a master TF central to responses to UV
581 radiation and blue light (Brown & Jenkins, 2008; Favory *et al.*, 2009; Gangappa & Botto, 2016), the
582 array of response patterns of transcript abundance and motif enrichment observed here indicate that
583 several TFs play key roles in downstream signaling leading to gene expression. In addition to HY5,
584 the known regulators of UV and blue light signaling and photomorphogenesis including PIF1, PIF3,
585 PIF4, PIF7 and BES1 (Hayes *et al.*, 2014; Gangappa & Botto, 2016; Pedmale *et al.*, 2016; Liang *et al.*
586 *et al.*, 2018; Wang *et al.*, 2018) were predicted to regulate gene expression in response to solar UV-B
587 through UVR8, and in response to solar blue through CRYs (Figure 7, cluster B). Our data also
588 indicate that HY5, PIFs, BES1, HAT5, WRKYs and many other TFs could regulate the expression
589 of genes responsive to UV-B or UV-A_{sw} and require both UVR8 and CRYs (Figure 7, clusters B, C,
590 D and G). This shows that both UVR8 and CRY signaling employ some of the same TFs for gene
591 expression. However, the multiple points of interaction for crosstalk between UV-B, UV-A_{sw}, UV-
592 A_{lw} and blue light signaling pathways downstream of UVR8, CRYs and other photoreceptors
593 remain to be explored.

594

595 **4.3 Implications and conclusions**

596

597 With few exceptions, gene expression in response to solar UV-B and UV-A_{sw} depended on UVR8,
598 while that in response to UV-A_{lw} and blue light depended on CRYs. Why the “UV-B
599 photoreceptor” UVR8 played a role in the perception of solar UV-A_{sw} can be explained by the
600 numbers of solar UV-B and UV-A_{sw} photons predicted to be absorbed by UVR8, a physico-
601 chemical mechanism. Our prediction of photons absorbed by UVR8 was made possible by the new
602 spectral absorbance data we report, demonstrating the usefulness of extending such measurements
603 far along the tails of absorption spectra. We also observed *in vitro* monomerization of UVR8 dimers

604 exposed to wavelengths between 300 and 335 nm but not when exposed to longer ones, extending
605 previous knowledge into longer wavelengths. This lack of monomerization may explain why UVR8
606 does not play an important role in the perception of UV-A_{lw}. Thus, we describe the mechanism by
607 which the steep slope of the solar spectrum in the UV region shifts perception of solar radiation by
608 UVR8 towards longer wavelengths than frequently assumed.

609

610 When considering both UVR8 and CRYs, we observed that the transcriptome-wide response
611 triggered by UV-B and UV-A_{sw} exposure was very strongly and negatively regulated by CRYs. The
612 reverse effect, modulation by UVR8 of gene expression in response to blue light was also observed
613 although it was much weaker. These results demonstrate for the first time the extent of the effect of
614 interactions downstream of UVR8 and CRYs on the transcriptome. These data also allowed us to
615 putatively identify several metabolic pathways affected by the interaction.

616

617 Specific groups of TFs were predicted *in silico* to control cascades of gene expression
618 corresponding to different patterns of transcriptome response to wavelengths across genotypes,
619 patterns which can only arise as the result of a complex signaling network including multiple points
620 of interaction downstream of UVR8 and CRYs. This prediction highlights that current models of
621 signaling downstream of UVR8 and CRYs, rather unsurprisingly, describe only the top portion of a
622 much deeper and ramified signaling network. As our study demonstrates, experiments combining
623 the use of multiple light treatments and multiple mutants in a factorial design allow teasing out
624 some of the signaling complexity that is missing from current models. The *in-silico* predictions we
625 report can guide the development of hypotheses about the mechanisms and players involved in
626 signaling, hypotheses that will need to be tested in future experiments.

627

628 As the wavelength boundaries for effective sensitivity of UVR8- and CRY-mediated perception of
629 sunlight do not coincide with the definitions of UV-B and UV-A radiation in common use (Björn,
630 2015), we consider that quantification of solar radiation based on these definitions is only
631 marginally useful when studying sunlight perception by plants, i.e., photomorphogenesis rather than
632 stress damage. Even more important, is that in both irradiation- and waveband-attenuation
633 experiments different regions within UV-A will trigger responses through different photoreceptors,
634 possibly resulting in contradictory or confusing results. In the present study, splitting the UV-A
635 waveband at 350 nm into UV-A_{sw} and UV-A_{lw} was the key to revealing the effective roles of UVR8
636 and CRYs in the perception of UV radiation in sunlight. Thus, as we routinely do for red and far-red

637 light in the visible, it is also very profitable to use plant-photomorphogenesis-specific waveband
638 definitions to characterize radiation in the UV-A region.

639

640 **6 ACKNOWLEDGEMENTS**

641

642 We acknowledge Petri Auvinen (University of Helsinki) for RNA-seq. Funding by Academy of
643 Finland (252548) to PJA, and (307335) to MB and JS; EDUFI Fellowship, Finnish Cultural
644 Foundation and Doctoral Program in Plant Sciences funding (University of Helsinki) to NR;
645 Knowledge foundation (20130164) and Swedish Research Council Formas (942-2015-516) to ÅS;
646 Strategic Young Researchers Recruitment Programme (Örebro University) to LOM.

647

648 **7 AUTHORSHIP**

649

650 PJA and LOM planned the research. NR, MB, ÅS, PJA, and LOM designed experiments. NR,
651 AO'H, DF, KR, FW, AVL, and LOM performed experiments. NR, OS, JS, PJA, and LOM
652 analyzed data. NR, PJA and LOM wrote the paper with contributions from MB, JS, ÅS, GIJ, and
653 TL. All authors commented and approved the manuscript. PJA and LOM contributed equally as
654 senior authors.

655

656

657 **References**

658

659 Ahmad M., Cashmore A.R. (1993). HY4 gene of *A. thaliana* encodes a protein with characteristics
660 of a blue-light photoreceptor. *Nature*, 366, 162–166.

661 Ambrosini G., Groux R., Bucher P. (2018). PWMScan: a fast tool for scanning entire genomes with
662 a position-specific weight matrix (J Hancock, Ed.). *Bioinformatics*, 34, 2483–2484.

663 Andrews S. (2014). FastQC A quality control tool for high throughput sequence data. Babraham
664 Bioinformatics. URL <https://www.bioinformatics.babraham.ac.uk/projects/fastqc/> [accessed 12 June
665 2019].

666 Aphalo P.J. (2015). The r4photobiology suite: spectral irradiance. *UV4Plants Bulletin*, 2015, 21–29.

667 Aphalo P.J. (2018). Exploring temporal and latitudinal variation in the solar spectrum at ground
668 level with the TUV model. *UV4Plants Bulletin*, 2018, 45–56.

669 Banerjee R., Schleicher E., Meier S., Viana R.M., Pokorny R., Ahmad M., Bittl R., Batschauer A.
670 (2007). The signaling state of Arabidopsis cryptochrome 2 contains flavin semiquinone. *The*
671 *Journal of Biological Chemistry*, 282, 14916–14922.

672 Björn L.O. (2015). History Ultraviolet-A, B, and C. *UV4Plants Bulletin*, 2015, 17–18.

673 Blomster T., Salojärvi J., Sipari N., Brosché M., Ahlfors R., Keinänen M., Overmyer K.,
674 Kangasjärvi J. (2011). Apoplastic reactive oxygen species transiently decrease auxin signaling and
675 cause stress-induced morphogenic response in Arabidopsis. *Plant Physiology*, 157, 1866–1883.

676 Bolger A.M., Lohse M., Usadel B. (2014). Trimmomatic: a flexible trimmer for Illumina sequence
677 data. *Bioinformatics*, 30, 2114–2120.

678 Bray N.L., Pimentel H., Melsted P., Pachter L. (2016). Near-optimal probabilistic RNA-seq
679 quantification. *Nature Biotechnology*, 34, 525–527.

680 Breilsford C.C., Morales L.O., Nezval J., Kotilainen T.K., Hartikainen S.M., Aphalo P.J., Robson
681 T.M. (2018). Do UV-A radiation and blue light during growth prime leaves to cope with acute high
682 light in photoreceptor mutants of *Arabidopsis thaliana*? *Physiologia Plantarum*, 165, 537–554.

683 Brown B.A., Cloix C., Jiang G.H., Kaiserli E., Herzyk P., Kliebenstein D.J., Jenkins G.I. (2005). A
684 UV-B-specific signaling component orchestrates plant UV protection. *Proceedings of the National*
685 *Academy of Sciences of the United States of America*, 102, 18225–18230.

686 Brown B.A., Jenkins G.I. (2008). UV-B signaling pathways with different fluence-rate response
687 profiles are distinguished in mature Arabidopsis leaf tissue by requirement for UVR8, HY5, and
688 HYH. *Plant Physiology*, 146, 576–588.

689 Christie J.M., Arvai A.S., Baxter K.J., Heilmann M., Pratt A.J., O'Hara A., Kelly S.M., Hothorn
690 M., Smith B.O., Hitomi K., *et al.* (2012). Plant UVR8 photoreceptor senses UV-B by tryptophan-
691 mediated disruption of cross-dimer salt bridges. *Science*, 335, 1492–1496.

692 Cloix C., Kaiserli E., Heilmann M., Baxter K.J., Brown B.A., O'Hara A., Smith B.O., Christie J.M.,
693 Jenkins G.I. (2012). C-terminal region of the UV-B photoreceptor UVR8 initiates signaling through
694 interaction with the COP1 protein. *Proceedings of the National Academy of Sciences of the United*
695 *States of America*, 109, 16366–16370.

696 Díaz-Ramos L.A., O'Hara A., Kanagarajan S., Farkas D., Strid Å., Jenkins G.I. (2018). Difference
697 in the action spectra for UVR8 monomerisation and *HY5* transcript accumulation in Arabidopsis.
698 *Photochemical and Photobiological Sciences*, 17, 1108–1117.

699 Emde C., Buras-Schnell R., Kylling A., Mayer B., Gasteiger J., Hamann U., Kylling J., Richter B.,
700 Pause C., Dowling T., *et al.* (2016). The libRadtran software package for radiative transfer
701 calculations (version 2.0.1). *Geoscientific Model Development*, 9, 1647–1672.

702 Favory J.-J., Stec A., Gruber H., Rizzini L., Oravec A., Funk M., Albert A., Cloix C., Jenkins G.I.,
703 Oakeley E.J., *et al.* (2009). Interaction of COP1 and UVR8 regulates UV-B-induced
704 photomorphogenesis and stress acclimation in Arabidopsis. *The EMBO Journal*, 28, 591–601.

705 Gangappa S.N., Botto J.F. (2016). The multifaceted roles of *HY5* in plant growth and development.
706 *Molecular Plant*, 9, 1353–1365.

707 Gasteiger E., Hoogland C., Gattiker A., Duvaud S., Wilkins M.R., Appel R.D., Bairoch A. (2005).
708 Protein identification and analysis tools on the ExPASy server. In *The Proteomics Protocols*
709 *Handbook*, pp. 571–607. Humana Press, Totowa, New Jersey.

710 Gruber H., Heijde M., Heller W., Albert A., Seidlitz H.K., Ulm R. (2010). Negative feedback
711 regulation of UV-B-induced photomorphogenesis and stress acclimation in Arabidopsis.
712 *Proceedings of the National Academy of Sciences of the United States of America*, 107, 20132–
713 20137.

714 Hayes S., Velanis C.N., Jenkins G.I., Franklin K.A. (2014). UV-B detected by the UVR8
715 photoreceptor antagonizes auxin signaling and plant shade avoidance. *Proceedings of the National*
716 *Academy of Sciences of the United States of America*, 111, 11894–11899.

717 Heijde M., Ulm R. (2013). Reversion of the Arabidopsis UV-B photoreceptor UVR8 to the
718 homodimeric ground state. *Proceedings of the National Academy of Sciences of the United States of*
719 *America*, 110, 1113–1118.

720 Holm S. (1979). A simple sequentially rejective multiple test procedure | BibSonomy. *Scandinavian*
721 *Journal of Statistics*, 6, 65–70.

- 722 Huang X., Ouyang X., Yang P., Lau O.S., Chen L., Wei N., Deng X.W. (2013). Conversion from
723 CUL4-based COP1-SPA E3 apparatus to UVR8-COP1-SPA complexes underlies a distinct
724 biochemical function of COP1 under UV-B. *Proceedings of the National Academy of Sciences of*
725 *the United States of America*, 110, 16669–16674.
- 726 Kaiserli E., Jenkins G.I. (2007). UV-B promotes rapid nuclear translocation of the Arabidopsis UV-
727 B specific signaling component UVR8 and activates its function in the nucleus. *The Plant Cell*, 19,
728 2662–2673.
- 729 Kallio M.A., Tuimala J.T., Hupponen T., Klemelä P., Gentile M., Scheinin I., Koski M., Käksi J.,
730 Korpelainen E.I. (2011). Chipster: user-friendly analysis software for microarray and other high-
731 throughput data. *BMC Genomics*, 12, 507.
- 732 Kerr J.B., Fioletov V.E. (2008). Surface ultraviolet radiation. *Atmosphere-Ocean*, 46, 159–184.
- 733 Khan A., Fornes O., Stigliani A., Gheorghe M., Castro-Mondragon J.A., van der Lee R., Bessy A.,
734 Chèneby J., Kulkarni S.R., Tan G., *et al.* (2018). JASPAR 2018: update of the open-access database
735 of transcription factor binding profiles and its web framework. *Nucleic Acids Research*, 46, D260–
736 D266.
- 737 Kleine T., Kindgren P., Benedict C., Hendrickson L., Strand Å. (2007). Genome-wide gene
738 expression analysis reveals a critical role for CRYPTOCHROME1 in the response of Arabidopsis
739 to high irradiance. *Plant Physiology*, 144, 1391–1406.
- 740 Kolde R. (2019). pheatmap: Pretty Heatmaps. R package version 1.0.12. URL [https://cran.r-](https://cran.r-project.org/web/packages/pheatmap/index.html)
741 [project.org/web/packages/pheatmap/index.html](https://cran.r-project.org/web/packages/pheatmap/index.html) [accessed 12 June 2019].
- 742 Lau K., Podolec R., Chappuis R., Ulm R., Hothorn M. (2019). Plant photoreceptors and their
743 signaling components compete for binding to the ubiquitin ligase COP1 using their VP-peptide
744 motifs. *The EMBO Journal*, 38, e102140.
- 745 Legendre P. (2018). lmodel2: Model II Regression. R package version 1.7-3. URL
746 <https://CRAN.R-project.org/package=lmodel2> [accessed 12 June 2019].
- 747 Lian H.L., He S.B., Zhang Y.C., Zhu D.M., Zhang J.Y., Jia K.P., Sun S.X., Li L., Yang H.Q.
748 (2011). Blue-light-dependent interaction of cryptochrome 1 with SPA1 defines a dynamic signaling
749 mechanism. *Genes and Development*, 25, 1023–1028.
- 750 Liang T., Mei S., Shi C., Yang Y., Peng Y., Ma L., Wang F., Li X., Huang X., Yin Y., *et al.* (2018).
751 UVR8 interacts with BES1 and BIM1 to regulate transcription and photomorphogenesis in
752 Arabidopsis. *Developmental Cell*, 44, 512–523.
- 753 Lin C. (2000). Plant blue-light receptors. *Trends in Plant Science*, 5, 337–342.

- 754 Lindfors A., Heikkilä A., Kaurola J., Koskela T., Lakkala K. (2009). Reconstruction of solar
755 spectral surface UV irradiances using radiative transfer simulations. *Photochemistry and*
756 *Photobiology*, 85, 1233–1239.
- 757 Liu H., Liu B., Zhao C., Pepper M., Lin C. (2011a). The action mechanisms of plant
758 cryptochromes. *Trends in Plant Science*, 16, 684–691.
- 759 Liu B., Yang Z., Gomez A., Liu B., Lin C., Oka Y. (2016). Signaling mechanisms of plant
760 cryptochromes in *Arabidopsis thaliana*. *Journal of Plant Research*, 129, 137–148.
- 761 Liu H., Yu X., Li K., Klejnot J., Yang H., Lisiero D., Lin C. (2008). Photoexcited CRY2 interacts
762 with CIB1 to regulate transcription and floral initiation in *Arabidopsis*. *Science*, 322, 1535–1539.
- 763 Liu B., Zuo Z., Liu H., Liu X., Lin C. (2011b). *Arabidopsis* cryptochrome 1 interacts with SPA1 to
764 suppress COP1 activity in response to blue light. *Genes and Development*, 25, 1029–1034.
- 765 Mazzella M.A., Cerdán P.D., Staneloni R.J., Casal J.J. (2001). Hierarchical coupling of
766 phytochromes and cryptochromes reconciles stability and light modulation of *Arabidopsis*
767 development. *Development*, 128, 2291–2299.
- 768 McCarthy D.J., Chen Y., Smyth G.K. (2012). Differential expression analysis of multifactor RNA-
769 Seq experiments with respect to biological variation. *Nucleic Acids Research*, 40, 4288–4297.
- 770 McLeay R.C., Bailey T.L. (2010). Motif Enrichment Analysis: a unified framework and an
771 evaluation on ChIP data. *BMC Bioinformatics*, 11, 165.
- 772 Morales L.O., Brosché M., Vainonen J., Jenkins G.I., Wargent J.J., Sipari N., Strid Å., Lindfors
773 A.V., Tegelberg R., Aphalo P.J. (2013). Multiple roles for UV RESISTANCE LOCUS8 in
774 regulating gene expression and metabolite accumulation in *Arabidopsis* under solar ultraviolet
775 radiation. *Plant Physiology*, 161, 744–759.
- 776 Neff M.M., Chory J. (1998). Genetic interactions between Phytochrome A, Phytochrome B, and
777 Cryptochrome 1 during *Arabidopsis* development. *Plant Physiology*, 118, 27–36.
- 778 O'Hara A., Jenkins G.I. (2012). In vivo function of tryptophans in the *Arabidopsis* UV-B
779 photoreceptor UVR8. *The Plant Cell*, 24, 3755–3766.
- 780 O'Malley R.C., Huang S.-S.C., Song L., Lewsey M.G., Bartlett A., Nery J.R., Galli M., Gallavotti
781 A., Ecker J.R. (2016). Cistrome and epicistrome features shape the regulatory DNA landscape. *Cell*,
782 165, 1280–1292.
- 783 Ohgishi M., Saji K., Okada K., Sakai T. (2004). Functional analysis of each blue light receptor,
784 cry1, cry2, phot1, and phot2, by using combinatorial multiple mutants in *Arabidopsis*. *Proceedings*
785 *of the National Academy of Sciences*, 101, 2223–2228.

786 Pedmale U.V., Huang S.C., Zander M., Cole B.J., Hetzel J., Ljung K., Reis P.A.B., Sridevi P., Nito
787 K., Nery J.R., *et al.* (2016). Cryptochromes interact directly with PIFs to control plant growth in
788 limiting blue light. *Cell*, 164, 233–245.

789 Pinheiro J., Bates D., DebRoy S., Sarkar D., R Core Team. (2018). nlme: Linear and Nonlinear
790 Mixed Effects Models. URL <https://cran.r-project.org/web/packages/nlme/index.html> [accessed 12
791 June 2019].

792 Podolec R., Ulm R. (2018). Photoreceptor-mediated regulation of the COP1/SPA E3 ubiquitin
793 ligase. *Current Opinion in Plant Biology*, 45, 18–25.

794 R Core Team. (2018). A language and environment for statistical computing. R Foundation for
795 Statistical Computing. URL <https://www.r-project.org/> [accessed 12 June 2019].

796 Rai N., Neugart S., Yan Y., Wang F., Siipola S.M., Lindfors A.V., Winkler J.B., Albert A., Brosché
797 M., Lehto T., *et al.* 2019. How do cryptochromes and UVR8 interact in natural and simulated
798 sunlight? *Journal of Experimental Botany*, 70, 4975–4990.

799 Ritchie M.E., Phipson B., Wu D., Hu Y., Law C.W., Shi W., Smyth G.K. (2015). limma powers
800 differential expression analyses for RNA-sequencing and microarray studies. *Nucleic Acids*
801 *Research*, 43, e47–e47.

802 Rizzini L., Favory J.-J., Cloix C., Faggionato D., O’Hara A., Kaiserli E., Baumeister R., Schäfer E.,
803 Nagy F., Jenkins G.I., *et al.* (2011). Perception of UV-B by the Arabidopsis UVR8 protein. *Science*,
804 332, 103–106.

805 Robinson M.D., McCarthy D.J., Smyth G.K. (2010). edgeR: a Bioconductor package for
806 differential expression analysis of digital gene expression data. *Bioinformatics*, 26, 139–140.

807 Sainsbury F., Thuenemann E.C., Lomonosoff G.P. (2009). pEAQ: versatile expression vectors for
808 easy and quick transient expression of heterologous proteins in plants. *Plant Biotechnology Journal*,
809 7, 682–693.

810 Sakai R., Winand R., Verbeiren T., Moere A.V., Aerts J. (2014). dendsort: modular leaf ordering
811 methods for dendrogram representations in R. *F1000Research* 3: 177.

812 Siipola S.M., Kotilainen T., Sipari N., Morales L.O., Lindfors A.V., Robson T.M., Aphalo P.J.
813 (2015). Epidermal UV-A absorbance and whole-leaf flavonoid composition in pea respond more to
814 solar blue light than to solar UV radiation. *Plant, Cell and Environment*, 38, 941–952.

815 Stracke R., Ishihara H., Huep G., Barsch A., Mehrrens F., Niehaus K., Weisshaar B. (2007).
816 Differential regulation of closely related R2R3-MYB transcription factors controls flavonol
817 accumulation in different parts of the *Arabidopsis thaliana* seedling. *The Plant Journal*, 50, 660–
818 677.

819 Wang W., Lu X., Li L., Lian H., Mao Z., Xu P., Guo T., Xu F., Du S., Cao X., *et al.* (2018).
820 Photoexcited CRYPTOCHROME1 interacts with dephosphorylated BES1 to regulate
821 brassinosteroid signaling and photomorphogenesis in Arabidopsis. *The Plant Cell*, 30, 1989–2005.
822 Wang H., Ma L.G., Li J.M., Zhao H.Y., Deng X.W. (2001). Direct interaction of Arabidopsis
823 Cryptochromes with COP1 in light control development. *Science*, 294, 154–158.
824 Wang Q., Zuo Z., Wang X., Gu L., Yoshizumi T., Yang Z., Yang L., Liu Q., Liu W., Han Y.-J., *et al.*
825 *al.* (2016). Photoactivation and inactivation of *Arabidopsis* cryptochrome 2. *Science*, 354, 343–347.
826 Warnes G.R., Bolker B., Lumley T., Johnson R.C. (2018). gmodels: Various R programming tools
827 for model fitting version 2.18.1 from CRAN. URL [https://cran.r-](https://cran.r-project.org/web/packages/gmodels/index.html)
828 [project.org/web/packages/gmodels/index.html](https://cran.r-project.org/web/packages/gmodels/index.html) [accessed 12 June 2019].
829 Wickham H. (2009). Ggplot2: elegant graphics for data analysis. Springer.
830 Wu D., Hu Q., Yan Z., Chen W., Yan C., Huang X., Zhang J., Yang P., Deng H., Wang J., *et al.*
831 (2012). Structural basis of ultraviolet-B perception by UVR8. *Nature*, 484, 214–219.
832 Yang Y., Liang T., Zhang L., Shao K., Gu X., Shang R., Shi N., Li X., Zhang P., Liu H. (2018).
833 UVR8 interacts with WRKY36 to regulate HY5 transcription and hypocotyl elongation in
834 Arabidopsis. *Nature Plants*, 4, 98–107.
835 Yang Z., Liu B., Su J., Liao J., Lin C., Oka Y. (2017). Cryptochromes orchestrate transcription
836 regulation of diverse blue light responses in plants. *Photochemistry and Photobiology*, 93, 112–127.
837 Yang X., Montano S., Ren Z. (2015). How does photoreceptor UVR8 perceive a UV-B Signal?
838 *Photochemistry and Photobiology*, 91, 993–1003.
839 Yang H.-Q., Tang R.-H., Cashmore A.R. (2001). The signaling mechanism of Arabidopsis CRY1
840 involves direct interaction with COP1. *The Plant Cell*, 13, 2573–2587.
841 Yu X., Liu H., Klejnot J., Lin C. (2010). The Cryptochrome blue light receptors. *The Arabidopsis*
842 *Book*, 8, e0135.
843 Zhang R., Calixto C.P.G., Marquez Y., Venhuizen P., Tzioutziou N.A., Guo W., Spensley M.,
844 Entizne J.C., Lewandowska D., Ten Have S., *et al.* (2017). A high quality Arabidopsis
845 transcriptome for accurate transcript-level analysis of alternative splicing. *Nucleic Acids Research*,
846 45, 5061–5073.
847 Zuo Z., Liu H., Liu B., Liu X., Lin C. (2011). Blue light-dependent interaction of CRY2 with SPA1
848 regulates COP1 activity and floral initiation in Arabidopsis. *Current Biology*, 21, 841–847.

849

850

851 **Figure legends:**

852

853 Figure 1. Transmittance of filters used in the outdoor experiment and the statistical contrasts
854 between pairs of filter treatments used to assess the effects of different ranges of wavelengths in
855 solar radiation.

856

857 Figure 2. Number of genes differentially expressed in response to 6 h of solar UV-B, UV-A and
858 blue radiation in (a) *Ler*, (b) *uvr8-2*, (c) *cry1cry2*. The Venn diagrams show the unique genes for
859 each waveband contrast and the overlap of genes between the waveband contrasts in each genotype.
860 The stacked bar plots show total number of genes responding to the waveband contrasts in each
861 genotype. The red bar refers to genes with increased expression and the blue bar refers to genes
862 with decreased expression. See Figure 1 for the contrasts used to assess the effects of UV-B, UV-A
863 and blue radiation. $FC > 1.5$ and $P_{\text{adjust}} < 0.05$.

864

865 Figure 3. Number of genes differentially expressed in response to 6 h of solar UV-A_{sw} and UV-A_{lw}
866 radiation in (a) *Ler*, (b) *uvr8-2*, (c) *cry1cry2*. The Venn diagrams show the unique genes for each
867 waveband contrast and the overlap of genes between the waveband contrasts in each genotype. The
868 stacked bar plots show total number of genes responding to the waveband contrasts in each
869 genotype. The red bar refers to genes with increased expression and the blue bar refers to genes
870 with decreased expression. See Figure 1 for the contrasts used to assess the effects of UV-A_{sw} and
871 UV-A_{lw} radiation. $FC > 1.5$ and $P_{\text{adjust}} < 0.05$.

872

873 Figure 4. Volcano plots showing DEGs with significantly increased expression (in red), DEGs with
874 significantly decreased expression (in blue) and not significant (in grey) in response to 6 h of solar
875 radiation of $\lambda < 350$ nm (290–350 nm) and $\lambda > 350$ nm (350–500 nm), λ refers to wavelength, n
876 refers to number of differentially expressed genes. See Figure 1 for the contrasts used to assess the
877 effects of $\lambda < 350$ nm and $\lambda > 350$ nm. $FC > 1.5$ and $P_{\text{adjust}} < 0.05$.

878

879 Figure 5. Estimates of solar UV-B, UV-A_{sw}, UV-A_{lw} and blue photons absorbed by UVR8 and
880 CRYs proteins throughout the day under the different filters used, expressed relative to their
881 respective daily maximum. The red horizontal lines show when the plants were moved outdoors
882 (0 h) or sampled (6 h and 12 h).

883

884 Figure 6. *In vitro* monomerization of purified UVR8 protein from *Nicotiana benthamiana* exposed
885 to UV radiation from a tunable laser. The time of exposure and photon doses at different
886 wavelengths were: 10 min and 1.9 μmol at 300 nm, 30 min and 5.1 μmol at 320 nm, 30 min and
887 4.5 μmol at 325 nm, 30 min and 3.8 μmol at 330 nm, 30 min and 3.4 μmol at 335 nm, 60 min and
888 6.2 μmol at 340 nm, 60 min and 5.8 μmol at 345 nm, 60 min and 5.3 μmol at 350 nm. The picture
889 shows the Coomassie stained gel. UVR8D refers to the dimer and UVR8M the monomer. The
890 figure is representative of three repeats.

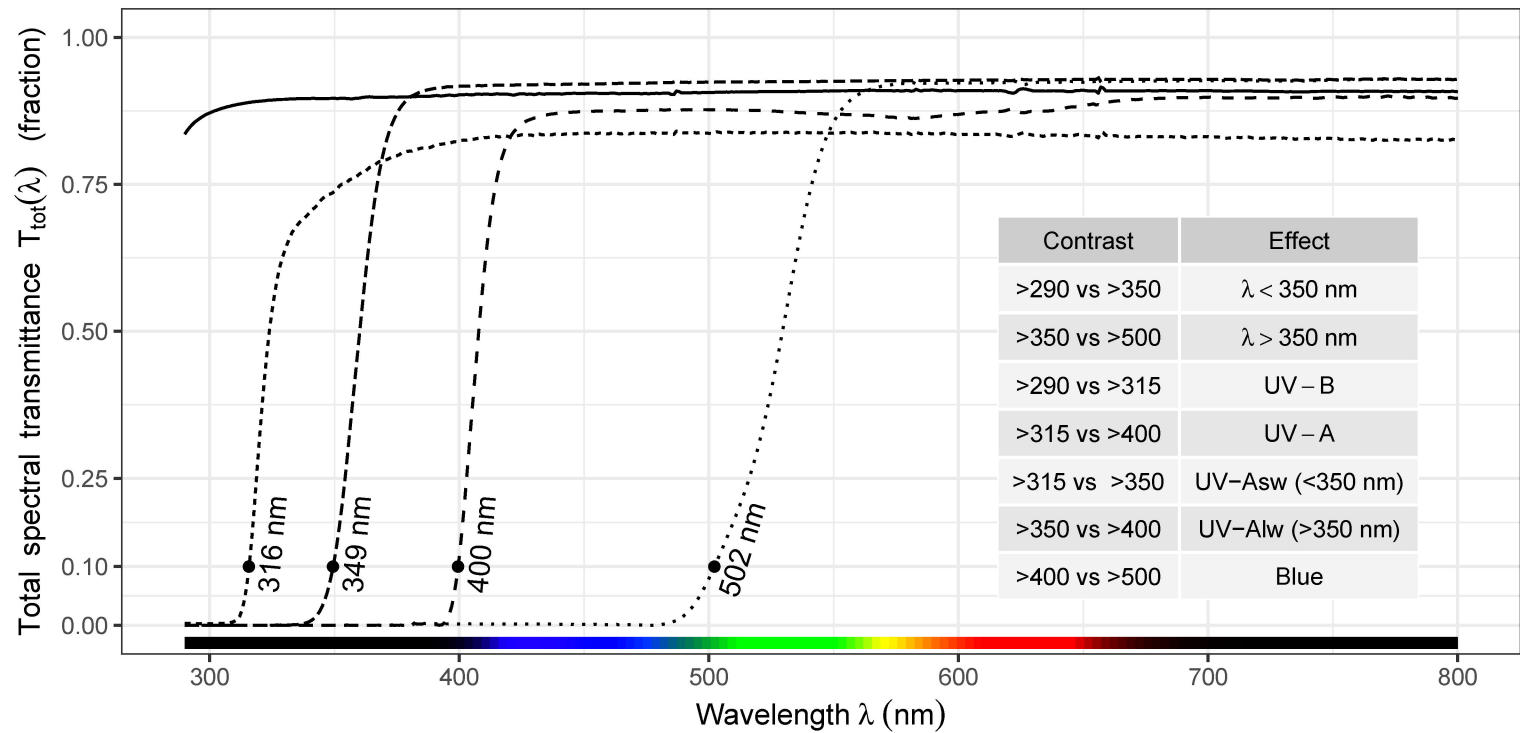
891

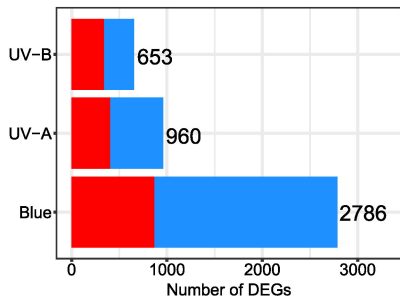
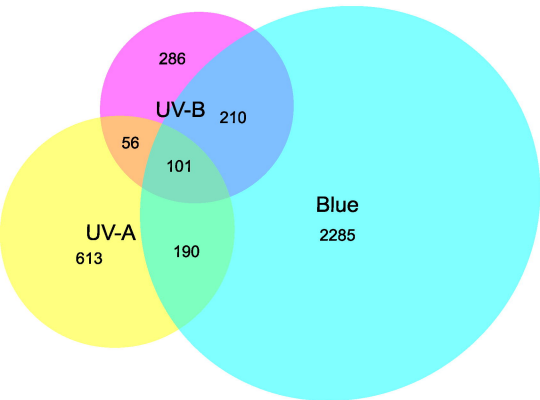
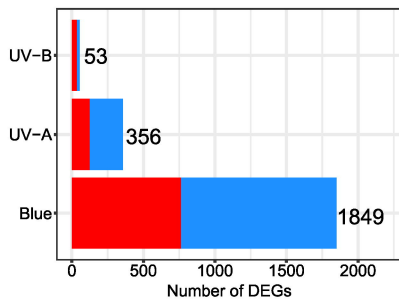
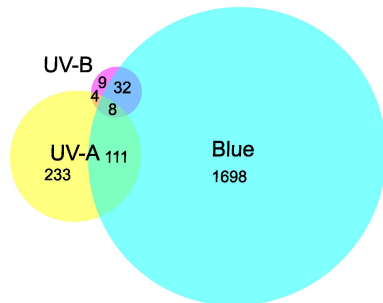
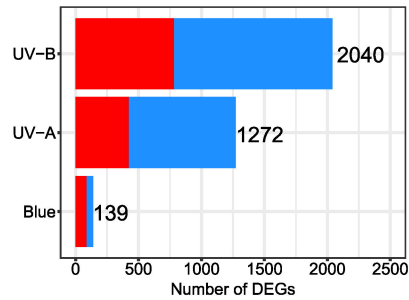
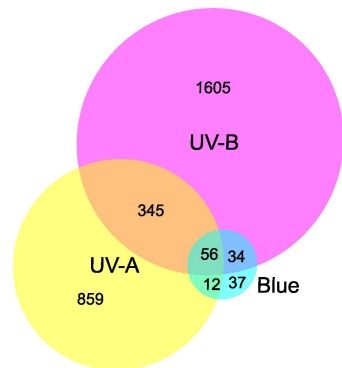
892 Figure 7. The *in silico* enrichment of DNA-binding motifs in our RNA-seq data showing 187
893 putative regulatory transcription factors (TFs). See Figure S8 for the position weight matrix of the
894 enriched motifs. The enrichments were done in 1000 base pairs upstream of the coding regions of
895 the DEGs from each waveband contrast and genotype combination. TFs with $P_{\text{adjust}} < 0.01$ in at
896 least one contrast and genotype combination were included in the figure. Of the 187 enriched TFs,
897 those which were also differentially expressed in our experiment are presented in bold letters and
898 shown as "DE" in the figure.

899

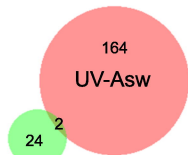
900 Figure 8. Transcript abundance ($\log_{10}\text{FC}$) of four genes *CHI*, *CHS*, *RUP2* and *SPS1* after 6 h and
901 12 h of treatment outdoors. These genes showed a significant triple interaction (genotype \times
902 radiation treatment \times exposure time). Mean $\pm 1\text{SE}$ from four biological replicates. The horizontal
903 bars show P_{adjust} values for pair-wise comparisons between treatments within each genotype. P_{adjust}
904 values for pair-wise contrasts are shown only in those panels where the overall effect of filter
905 treatment within a genotype and time point was significant (see Table S2).

Filter cut-off designations: — >290 ····· >315 - - - >350 - - - >400 ····· >500

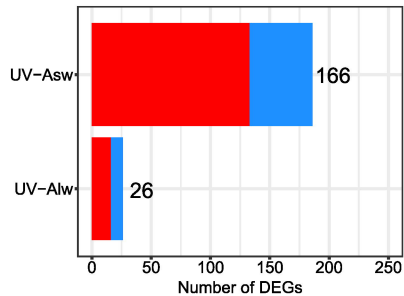


(a) *Ler***(b)** *uvr8-2***(c)** *cry1cry2*

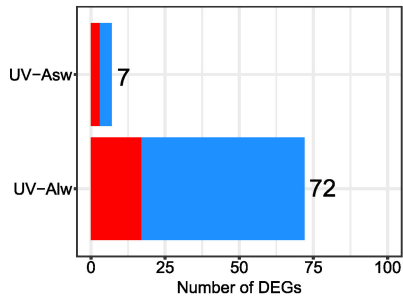
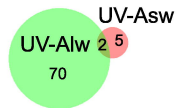
(a) Ler



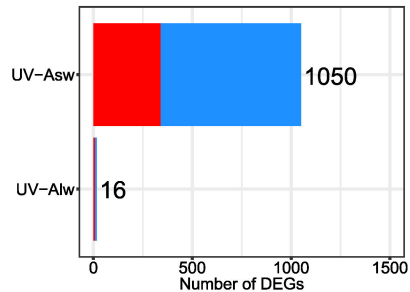
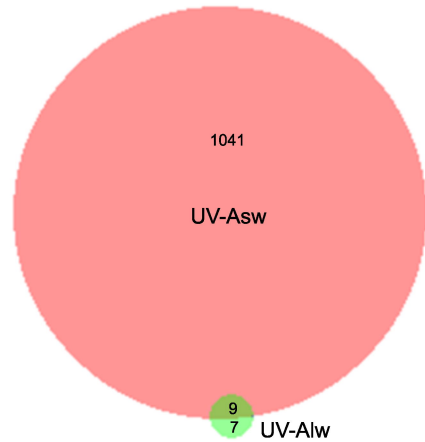
UV-Alw

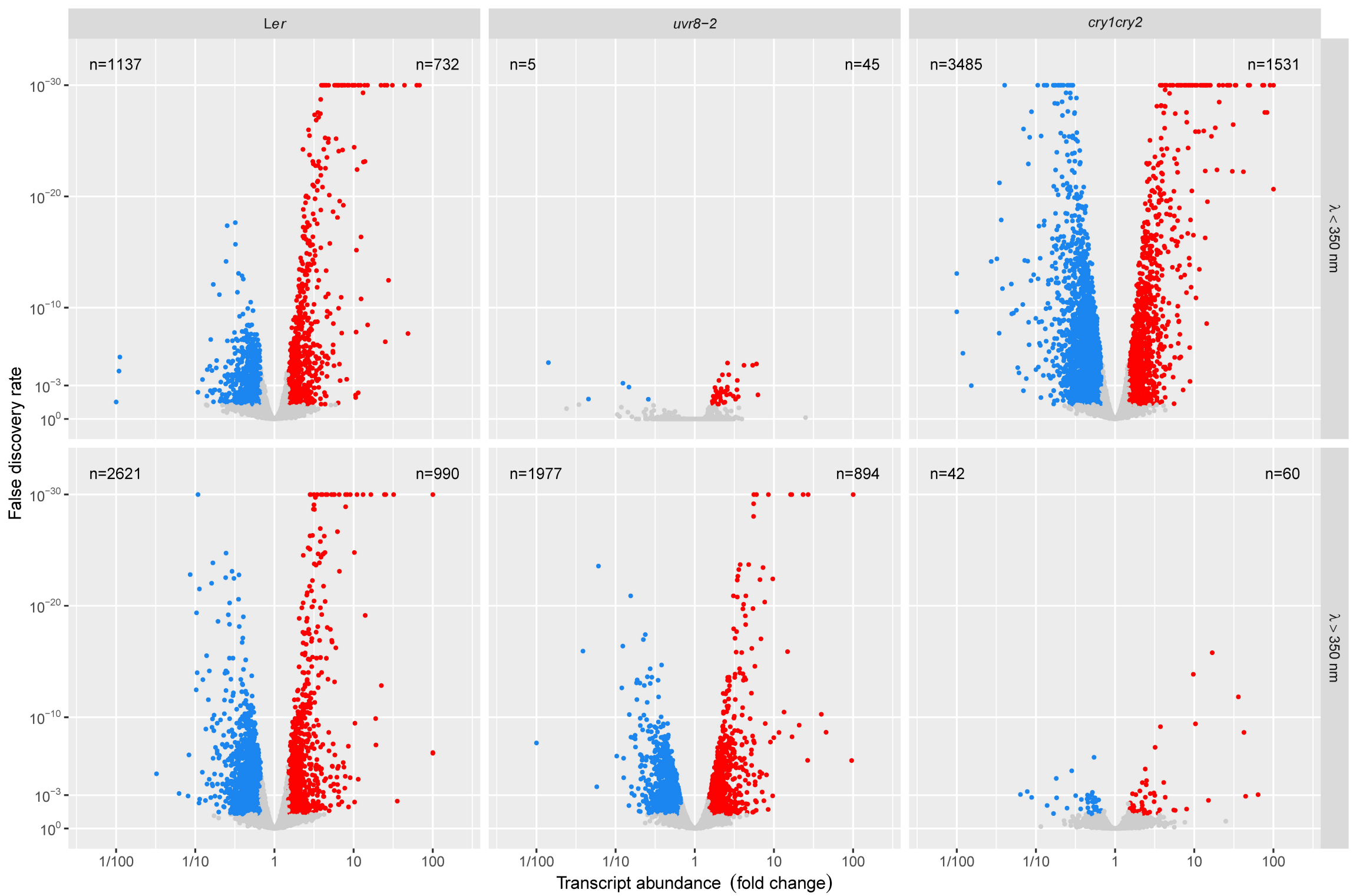


(b) *uvr8-2*



(c) *cry1cry2*





Filter cut-off wavelength (nm) — >290 - - - >315 - - - >350 - - - >400 ····· >500

